Tumbling of small axisymmetric particles in random and turbulent flows

K. Gustavsson, J. Einarsson, and B. Mehlig

Department of Physics, Gothenburg University, 41296 Gothenburg, Sweden

We analyse the tumbling of small non-spherical, axisymmetric particles in random and turbulent flows. We compute the orientational dynamics in terms of a perturbation expansion in the Kubo number, and obtain the tumbling rate in terms of Lagrangian correlation functions. These capture preferential sampling of the fluid gradients which in turn can give rise to differences in the tumbling rates of disks and rods. We show that this is a weak effect in Gaussian random flows. But in turbulent flows persistent regions of high vorticity cause disks to tumble much faster than rods, as observed in direct numerical simulations [Parsa *et al.*, Phys. Rev. Lett. **109** (2012) 134501]. For larger particles (at finite Stokes numbers), rotational and translational inertia affects the tumbling rate and the angle at which particles collide, due to the formation of rotational caustics.

The orientational dynamics of axisymmetric particles in random and turbulent flows is of great significance in many areas of the Natural Sciences and in technology. For example, turbulent flow visualisation experiments employ reflective flakes [1]. Patterns of non-spherical particles suspended in flows were investigated in [2–4], revealing singularities in the orientational patterns of rheoscopic suspensions. Aerosols in the natural world are often suspensions of small non-spherical particles. For example, tumbling ice particles in turbulent clouds may play an important role in cloud-particle interactions [5]. Small dust grains in circumstellar accretion disks are not spherically symmetric [6, 7]. The relative orientation at which such grains collide may have important consequences for the outcomes of grain-grain collisions, and their orientation may have important implications for photophoretic forcing [8]. A last example concerns plankton in the upper ocean layer. Their tumbling may influence their nutrient uptake and light scattering [9].

In all of these cases the particles are smaller than the smallest turbulent eddies in the suspending flow, and the orientational dynamics of such small particles is driven by the local flow gradients: the difference in flow velocity over the particle leads to a hydrodynamic torque. Understanding how small non-spherical particles respond to flow gradients is a necessary step in describing the collision dynamics of turbulent suspensions of axisymmetric particles. Morever, the orientational dynamics of small non-spherical particles is of fundamental interest in turbulence research, because it reflects the statistics of the velocity gradients in turbulent flows [10]. Recently, the tumbling rate of small axisymmetric particles in turbulent flows was investigated experimentally and by direct numerical simulations [12]. It was found that disks tumble, on average, at a much higher rate than rods. This was related to the observation that rods tend to preferentially align with the vorticity of the flow [10]. But disks too exhibit alignment with flow structures, the equations of motion for disks and rods are in fact almost the same. The only difference is that the flow-gradient matrix for

rods is replaced by its negative transpose for disks (explained in more detail below).

This raises the questions: which flow configurations are responsible for the difference in tumbling between disks and rods? How do disks align? How does the tumbling in turbulent flows differ from that in random flows, how sensitive is the orientational dynamics to particular features of turbulent flows? How does the nature of the turbulent Lagrangian flow statistics influence the tumbling? How does tumbling reflect vorticity? Finally, what is the effect of particle inertia upon the tumbling?

To answer these questions we analyse the tumbling of small non-spherical particles in random and turbulent flows using perturbation theory. In the simplest case our problem is governed by three dimensionless parameters. The Kubo number $\mathrm{Ku} = u_0\tau/\eta$ is a dimensionless measure of the correlation time of the flow, here u_0, τ and η are the smallest characteristic speed-, time- and length scales of the flow (Kolmogorov scales in turbulence). The Stokes number, St, characterises the damping of the particle dynamics with respect to the flow. The third parameter is the aspect ratio λ of the axisymmetric particle.

In the limit of St $\to 0$, the orientational dynamics does not affect the translational motion: the centre-of-mass $\boldsymbol{r}$ is simply advected. The orientational dynamics of the unit vector $\boldsymbol{n}$ pointing along the symmetry axis of the particle is driven by the local flow gradients (provided that the dimensions of the particle are much smaller than η). In other words $\boldsymbol{n}$ follows Jeffery's equation [11]. We use dimensionless units $t = \tau t'$, $\boldsymbol{r} = \eta \boldsymbol{r}'$, $\boldsymbol{u} = u_0 \boldsymbol{u}'$. Dropping the primes, the equation of motion reads:

$$\dot{\boldsymbol{r}} = \mathrm{Ku}\,\boldsymbol{u}\,, \quad \dot{\boldsymbol{n}} = \mathrm{Ku}\left[\mathbb{O}\boldsymbol{n} + \Lambda\left(\mathbb{S}\boldsymbol{n} - (\boldsymbol{n}^{\mathrm{T}}\mathbb{S}\boldsymbol{n})\boldsymbol{n}\right)\right]\,. \quad (1)$$

Here $\Lambda = (\lambda^2 - 1)/(\lambda^2 + 1)$ parameterises the particle shape ($\Lambda = -1$ for disks, 0 for spheres, and 1 for rods). Further $\mathbb{S} = (\mathbb{A} + \mathbb{A}^{\mathrm{T}})/2$ and $\mathbb{O} = (\mathbb{A} - \mathbb{A}^{\mathrm{T}})/2$ are the symmetric and antisymmetric parts of the matrix $\mathbb{A}(\boldsymbol{r}_t, t)$ of flow gradients. The time-averaged tumbling rate $\langle \dot{n}^2 \rangle$ is determined by the fluctuations of $\mathbb{S}(\boldsymbol{r}_t, t)$ and $\mathbb{O}(\boldsymbol{r}_t, t)$ along the particle trajectories $\boldsymbol{r}_t$. In the limit of rapidly

fluctuating random flows (Ku → 0) the tumbling rate averaged along trajectories can be replaced by an average over the ensemble of $\mathbb{S}$ and $\mathbb{O}$. This average, denoted by $\langle \dot{n}^2 \rangle_0$, is determined by the invariants of $\mathbb{S}$ and $\mathbb{O}$. For incompressible, isotropic random flows one finds:

$$\langle \dot{n}^2 \rangle \approx \langle \dot{n}^2 \rangle_0 = \text{Ku}^2\big(-5\text{Tr}\,\langle \mathbb{O}^2 \rangle + 3\Lambda^2 \text{Tr}\,\langle \mathbb{S}^2 \rangle\big)/15\,. \quad (2)$$

Note that in homogenous flows $\text{Tr}\langle \mathbb{S}^2 \rangle = -\text{Tr}\langle \mathbb{O}^2 \rangle = \text{Tr}\langle \mathbb{A}^{\text{T}}\mathbb{A} \rangle/2$. In turbulent flows $\text{Tr}\langle \mathbb{A}^{\text{T}}\mathbb{A} \rangle$ is proportional to the energy dissipation. An expression equivalent to (2) was first derived in [13] and is also quoted in [12]. Eq. (2) is symmetric in Λ, meaning that disks tumble at the same rates as rods. Differences between disks and rods could arise for two reasons. First, one or more symmetries may be broken. For example, breaking isotropy [14] gives rise to an extra term that is odd in Λ. Second, in homogenous, isotropic, and incompressible flows differences in the behaviour of disks and rods may arise due to preferential sampling of the flow gradients.

The dynamics of small disks and rods are closely related. Taking the limits $\lambda \to 0$ and $\lambda \to \infty$ in Eq. (1) shows that the unnormalised orientation vectors $\boldsymbol{q}$ (such that $\boldsymbol{n} = \boldsymbol{q}/|\boldsymbol{q}|$) of disks and rods obey $\dot{\boldsymbol{q}}_{\text{disk}} = -\text{Ku}\,\mathbb{A}^{\text{T}}\boldsymbol{q}_{\text{disk}}$ and $\dot{\boldsymbol{q}}_{\text{rod}} = \text{Ku}\,\mathbb{A}\boldsymbol{q}_{\text{rod}}$. In persistent flow regions, the dynamics $\boldsymbol{q}(t)$ is determined by the eigenvectors of $-\mathbb{A}^{\text{T}}$ or of $\mathbb{A}$. If all eigenvalues of $\mathbb{A}$ are real, rods align with the eigenvector corresponding to the largest eigenvalue. If $\mathbb{A}$ has one real and two complex conjugate eigenvalues, rods align if the real eigenvalue is positive and tumble otherwise. Changing $\mathbb{A} \to -\mathbb{A}^{\text{T}}$ (rods to disks) switches the signs of the eigenvalues. Therefore, when $\mathbb{A}$ has complex eigenvalues the transformation $\mathbb{A} \to -\mathbb{A}^{\text{T}}$ alters the dynamics from tumbling to aligning, and vice versa. The eigenvalues of $\mathbb{A}$ are parameterised by the invariants $\text{Tr}\mathbb{A}^2$ and $\text{Tr}\mathbb{A}^3$ [15]. In turbulent flows the joint distribution of $\text{Tr}\mathbb{A}^2$ and $\text{Tr}\mathbb{A}^3$ is known to be strongly skewed [16]. The resulting asymmetry under $\text{Tr}\mathbb{A}^3 \to -\text{Tr}\mathbb{A}^3$ in the distribution of flow gradients causes different tumbling rates for rods and disks in persistent flows.

This argument explains why rods and disks tumble differently in persistent flow regions, where the flow gradient matrix $\mathbb{A}$ remains approximately constant while $\boldsymbol{n}$ aligns. In turbulent flows, however, the matrix $\mathbb{A}$ may change on the same time scale as $\boldsymbol{n}$. The resulting time-dependent problem is very difficult to solve. Below we attack the problem from a different point of view: in the limit of rapidly changing flows we express the tumbling rate in terms of the Lagrangian fluctuations of $\mathbb{A}$. The orientational dynamics may be computed by iterating the implicit solution of (1):

$$\boldsymbol{n}_{t'} = \boldsymbol{n}_0 + \text{Ku}\int_0^{t'}\text{d}t\,[\mathbb{O}_t\boldsymbol{n}_t + \Lambda(\mathbb{S}_t\boldsymbol{n}_t - (\boldsymbol{n}_t^{\text{T}}\mathbb{S}_t\boldsymbol{n}_t)\boldsymbol{n}_t)]\,. \quad (3)$$

Here $\mathbb{O}_t \equiv \mathbb{O}(\boldsymbol{r}_t, t)$ and $\mathbb{S}_t \equiv \mathbb{S}(\boldsymbol{r}_t, t)$. Iteratively substituting $\boldsymbol{n}_t$ into the r.h.s. of (3) generates perturbation
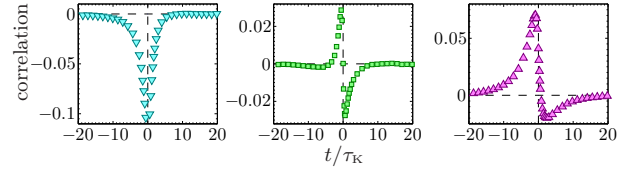

FIG. 1: *(Color online).* Numerical results for Lagrangian correlations $\text{Tr}\langle \mathbb{S}_0^2 \mathbb{S}_t \rangle \tau_{\text{K}}^3$ (cyan,▽), $\langle \text{Tr}\mathbb{S}_0\mathbb{O}_0\mathbb{S}_t \rangle \tau_{\text{K}}^3$ (green,□) and $\text{Tr}\langle \mathbb{O}_0^2 \mathbb{S}_t \rangle \tau_{\text{K}}^3$ (magenta,△). Obtained using the JHU turbulence data set [17, 18], see text. In units of $\tau_{\text{K}} \equiv 1/\sqrt{\text{Tr}\langle \mathbb{A}^{\text{T}}\mathbb{A} \rangle}$.

expansions for $\boldsymbol{n}_t$ and $\dot{\boldsymbol{n}}_t$ in powers of Ku. Averaging gives us the leading-order correction to Eq. (2)

$$\langle \dot{n}^2 \rangle = \langle \dot{n}^2 \rangle_0 + \frac{2}{5}\text{Ku}^3\Lambda\int_0^\infty\text{d}t \quad (4)$$

$$\times\big[-\text{Tr}\,\langle \mathbb{O}_0^2\mathbb{S}_{-t} \rangle + 2\Lambda\text{Tr}\,\langle \mathbb{S}_0\mathbb{O}_0\mathbb{S}_{-t} \rangle + \frac{3}{7}\Lambda^2\text{Tr}\,\langle \mathbb{S}_0^2\mathbb{S}_{-t} \rangle\big]\,.$$

This correction is given by three-point Lagrangian correlation functions of $\mathbb{O}_t$ and $\mathbb{S}_t$.

Eq. (4) shows that the Ku^3-correction to Eq. (2) contains terms antisymmetric in Λ, causing disks to tumble differently from rods. For Gaussian random flows, the Lagrangian correlation functions in the integrands of (4) can be calculated analytically for small Ku, as we show below. For turbulent flows we have determined the correlation functions numerically, using data from the JHU turbulence data set [17, 18].

Random flows. We represent the incompressible, homogenous, and isotropic random flow as $\boldsymbol{u}(\boldsymbol{r}, t) = \nabla \wedge \boldsymbol{A}(\boldsymbol{r}, t)$ in terms of a Gaussian random vector potential $\boldsymbol{A}(\boldsymbol{r}, t)$ with zero mean and correlation function $\langle A_i(\boldsymbol{r}_0, 0)A_j(\boldsymbol{r}_0, t) \rangle = \delta_{ij}\exp(-|t|)/6$ [19]. The corresponding Eulerian correlation functions (evaluated at a fixed point $\boldsymbol{r}_0$ in space) are given by $\text{Tr}\langle \mathbb{S}(\boldsymbol{r}_0, 0)\mathbb{S}(\boldsymbol{r}_0, t) \rangle = -\text{Tr}\langle \mathbb{O}(\boldsymbol{r}_0, 0)\mathbb{O}(\boldsymbol{r}_0, t) \rangle = 5\,e^{-|t|}/2$. The Eulerian three-point functions vanish because the Gaussian gradient distribution is even. The Lagrangian correlations at finite values of Ku can be computed perturbatively, taking into account recursively that the actual trajectory $\boldsymbol{r}_t$ deviates from its initial condition $\boldsymbol{r}_0$. As shown in [20, 21] this yields an expansion in Ku.

The Lagrangian correlation functions quantify the degree of preferential sampling. As Eq. (4) shows differences in tumbling rates between disks and rods are determined by Lagrangian three-point correlations. We find to third order in Ku:

$$\text{Tr}\langle \mathbb{S}_0\mathbb{O}_0\mathbb{S}_t \rangle = \frac{35\text{Ku}^3}{16}\text{sgn}(t)e^{-|t|}(1 - 2|t|e^{-|t|} - e^{-2|t|})\,,$$

$$\text{Tr}\langle \mathbb{O}_0\mathbb{O}_0\mathbb{S}_t \rangle = -\frac{125\text{Ku}^3}{288}\text{sgn}(t)e^{-|t|}(1 - 2|t|e^{-|t|} - e^{-2|t|})\,,$$

$$\text{Tr}\langle \mathbb{S}_0^2\mathbb{S}_t \rangle = -\frac{175\text{Ku}^3}{96}\text{sgn}(t)e^{-|t|}(1 - 2|t|e^{-|t|} - e^{-2|t|})\,. \quad (5)$$

Thus the Lagrangian flow-gradient fluctuations are not Gaussian, a consequence of preferential sampling at finite Kubo numbers. Extending (4) to Ku^6 and inserting the required correlation functions [such as (5)] we obtain:

$$\langle \dot{n}^2 \rangle = \frac{\text{Ku}^2}{6}(5 + 3\Lambda^2) - \frac{\text{Ku}^4}{4}\Lambda^2(5 + 3\Lambda^2) \quad (6)$$
$$+ \frac{\text{Ku}^6}{864}\Lambda(-25 + 4668\Lambda + 45\Lambda^2 + 7236\Lambda^3 + 2484\Lambda^5) + \cdots.$$

Odd powers in Λ occur in this expression, giving rise to differences in tumbling between disks and rods. But the effect is weak, it occurs to order Ku^6. Eq. (6) (extended to order Ku^8) can be resummed by Padé-Borel resummation [21], yielding accurate results up to $\text{Ku} \sim 1$.

We conclude that disks and rods tumble at almost the same rates in Gaussian random flows. The question is thus what causes the striking differences between the dynamics of rods and disks observed in [12]?

Turbulent flows. According to Eq. (4), differences in the tumbling of rods and disks due to preferential sampling of the flow gradients are parameterised by Lagrangian three-point correlation functions. We cannot compute these correlation functions analytically, and have thus evaluated them numerically using the JHU turbulence data set [17, 18]. The data set contains a direct numerical simulation of forced, isotropic turbulence on a 1024^3 grid, for circa 45 Kolmogorov times τ_{K}, at a Taylor micro-scale Reynolds number $\text{Re}_\lambda = 433$. From the data set we computed the Lagrangian correlations. The three correlation functions contributing to the tumbling rate in Eq. (4) are shown in Fig. 1. The major contribution after integration comes from the $\text{Tr}\langle \mathbb{O}_0^2 \mathbb{S}_{-t} \rangle$-term, with the contribution of the $\text{Tr}\langle \mathbb{S}_0^2 \mathbb{S}_{-t} \rangle$-term approximately a factor $\Lambda^2/3$ smaller. These two terms together result in a substantial contribution to the tumbling rate that is odd in Λ, giving rise to pronounced differences in the tumbling of rods and disks.

We have presented arguments valid for persistent flows (large Ku), as well as the perturbative small-Ku result (4). We now show that the conclusions drawn from the two arguments are closely connected. In turbulence large positive values of $\text{Tr}\mathbb{A}^3$ typically coincide with large negative values of $\text{Tr}\mathbb{A}^2$ (vortex-dominated flow) [16, 22]. Conversely, negative values of $\text{Tr}\mathbb{A}^3$ typically coincide with positive $\text{Tr}\mathbb{A}^2$ (strain-dominated flow). We decompose $\text{Tr}\mathbb{A}^3 = 3\text{Tr}\mathbb{O}^2\mathbb{S} + \text{Tr}\mathbb{S}^3$, and note that in turbulence $\text{Tr}\langle \mathbb{O}^2\mathbb{S} \rangle > 0$ and $\text{Tr}\langle \mathbb{S}^3 \rangle < 0$ (see Fig. 1). Thus, large positive values of $\text{Tr}\mathbb{A}^3$ typically correspond to large values of $\text{Tr}\mathbb{O}^2\mathbb{S}$. The corresponding flow regions are vortex tubes [23] that persist long enough for rods to align and disks to tumble. The differences in the tumbling rates of disks and rods due to such persistent regions are reflected in the integral over $\text{Tr}\mathbb{O}_0^2\mathbb{S}_{-t}$ in Eq. (4): first a local strain creates the vortex tube. This takes several τ_{K} (Fig. 1, right panel). During this time rods and disks

align in different ways, and after that disks start to rotate. Strain-dominated flow regions, by contrast, correspond to large negative values of $\text{Tr}\mathbb{S}^3$ and the differences in tumbling rates result in the integral over $\text{Tr}\mathbb{S}_0^2\mathbb{S}_{-t}$ in Eq. (4). In this case the difference between rods and disks is due to the difference in magnitude of eigenvalues. Since the middle eigenvalue of $\mathbb{A}$ is positive on average, and the sum of eigenvalues is zero, the magnitude of the first eigenvalue (acting on the rod) is necessarily smaller than that of the last (acting on the disk): disks to respond more quickly than rods to strain-dominated regions and hence exhibit a larger tumbling rate also in these regions.

Fig. 2 (left) shows how $\dot{n}^2$ varies as a function of time in a turbulent flow $\boldsymbol{u}(\boldsymbol{r}, t)$. Also shown is $\text{Tr}\mathbb{O}_t^2\mathbb{S}_t$. In agreement with the calculations and arguments outlined above, rods align and disks tumble strongly when $\text{Tr}\mathbb{O}_t^2\mathbb{S}_t$ is large and positive. Fig. 2 (right) shows numerical results for $\langle \dot{n}^2 \rangle$ in a turbulent flow, as a function of the aspect ratio λ. The numerical simulations are compared to the theoretical result (4) with correlation functions according to Fig. 1. Eq. (4) is valid for small Ku and general values of Λ. In turbulence $\text{Ku} \sim 1$, and the numerical tumbling rate $\langle \dot{n}^2 \rangle$ is not expected to agree quantitatively with Eq. (4). In other contexts we have found that the parameter-dependence (in this case the Λ-dependence) in Ku-expansions is often approximately independent of Ku for small and intermediate Ku. This may explain why the general shape of the curve shown in Fig. 2 is approximately correct, but not the amplitude.

Also shown in Fig. 2 is $\dot{n}^2$ averaged conditional on large $\text{Tr}\mathbb{O}^2\mathbb{S}$: the substantial difference in tumbling rates of disks and rods is largely caused by the flow configurations with large $\text{Tr}\mathbb{O}^2\mathbb{S}$, confirming the picture outlined above. Finally, when rods align with the leading eigenvector of $\mathbb{A}$, then the vorticity vector $\boldsymbol{\Omega} = (\boldsymbol{\nabla} \wedge \boldsymbol{u})/2$ does the same. But for disks $\boldsymbol{n}$ is preferentially orthogonal to $\boldsymbol{\Omega}$ (inset of right panel of Fig. 2). This is expected since the equations of motion for rods and vorticity have a common term involving $\mathbb{A}$ [10, 24].

Effects of particle inertia. When $\text{St} > 0$, different moments of inertia and fluid resistance tensors result in differences in the tumbling of disks and rods. Neglecting possible effects due to the unsteadiness of the flow, the dynamics of small spheroidal particles at finite St is

$$\dot{\boldsymbol{r}} = \text{Ku}\,\boldsymbol{v}\,, \qquad \dot{\boldsymbol{n}} = \text{Ku}\,\boldsymbol{\omega} \wedge \boldsymbol{n} \quad (7)$$
$$\text{St}\,\dot{\boldsymbol{v}} = \left[C_\perp^{(t)}\mathbb{I} + \left(C_\parallel^{(t)} - C_\perp^{(t)} \right)\boldsymbol{n}\boldsymbol{n}^{\text{T}} \right](\boldsymbol{u} - \boldsymbol{v})$$
$$\text{St}\,\dot{\boldsymbol{\omega}} = \left[C_\perp^{(r)}\mathbb{I} + \left(C_\parallel^{(r)} - C_\perp^{(r)} \right)\boldsymbol{n}\boldsymbol{n}^{\text{T}} \right](\boldsymbol{\Omega} - \boldsymbol{\omega})$$
$$- \Lambda C_\perp^{(r)}(\mathbb{S}\boldsymbol{n}) \wedge \boldsymbol{n} + \text{Ku}\,\text{St}\,\Lambda(\boldsymbol{n} \cdot \boldsymbol{\omega})\boldsymbol{\omega} \wedge \boldsymbol{n}\,.$$

Here St is the Stokes number of a spherical particle of radius equal to the minor axis of the spheroidal particle, $\mathbb{I}$ is the unit matrix, and the coefficients C are given by
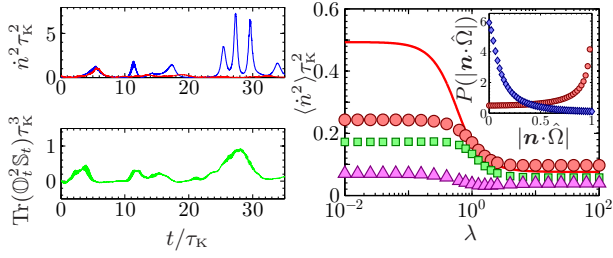
FIG. 2: *(Color online).* Left: Tumbling rate $\dot{n}^2$ for a disk (blue) and a rod (red) in turbulent flow as a function of time, using the JHU turbulence data set [17, 18]. Also shown is $\mathrm{Tr}\,\mathbb{O}_t^2\mathbb{S}_t$ (green). Right: average squared tumbling rate $\langle\dot{n}^2\rangle$ in turbulence as a function of the aspect ratio λ (red,○). Eq. (4) with data from Fig. 1 is shown as solid red. Also shown is $\dot{n}^2$ averaged conditional on large values of $\mathrm{Tr}\,\mathbb{O}_t^2\mathbb{S}_t$ (green,□) (23% of the sampled data) conditional on small values of $\mathrm{Tr}\,\mathbb{O}_t^2\mathbb{S}_t$ (magenta,△) (77% of the sampled data). Inset: alignment distributions for disks (blue,◇) and rods (red,○).

FIG. 3: *(Color online).* Left: $\langle\dot{n}^2\rangle$ as a function of St in a Gaussian random flow (see text). Symbols show results of numerical simulations, solid lines show theory (9). Parameters: Ku = 0.1, $\lambda = \sqrt{0.1}$ (blue,◇), $\lambda = 1$ (green,□), $\lambda = \sqrt{10}$ (red,○). Right: distribution of the relative angle $\Delta\varphi$ between the orientation vectors $\boldsymbol{n}$ of two particles close together (at separation $R = 0.1\eta$). Black dashed shows $\sin\Delta\varphi$. Parameters: Ku = 1, $\lambda = \sqrt{10}$. St = 0 (cyan, ▽), St = 1 (green, □) and St = 10 (magenta, △).

translational ($C^{(t)}$) and rotational ($C^{(r)}$) hydrodynamic drag [25] and moment of inertia along ($C_\parallel$) and perpendicular ($C_\perp$) to the particle symmetry axis:

$$C_\perp^{(t)} = \frac{8(\lambda^2-1)}{3\lambda((2\lambda^2-3)\beta+1)}, \; C_\parallel^{(t)} = \frac{4(\lambda^2-1)}{3\lambda((2\lambda^2-1)\beta-1)},$$
$$C_\perp^{(r)} = \frac{40(\lambda^2-1)}{9\lambda((2\lambda^2-1)\beta-1)}, \; C_\parallel^{(r)} = \frac{20(\lambda^2-1)}{9\lambda(1-\beta)},$$
$$\beta = \frac{1}{\lambda\sqrt{|\lambda^2-1|}} \begin{cases} \mathrm{acos}(\lambda) & \text{if } \lambda \le 1 \\ \mathrm{acosh}(\lambda) & \text{if } \lambda > 1 \end{cases}. \quad (8)$$

Eqs. (7) and (8) are widely used in the engineering literature, see for example [26] and references therein. In the limit St $\to 0$, Eq. (1) is recovered.

The tumbling rate resulting from (7) can be computed in a small-Ku perturbation theory, analogous to our treatment of Eq. (1) outlined above. To lowest order in Ku we find for a spheroid in the random-flow model:

$$\langle\dot{n}^2\rangle = \frac{\mathrm{Ku}^2}{6} \frac{C_\perp^{(r)}(5+3\Lambda^2)}{\mathrm{St}+C_\perp^{(r)}}. \quad (9)$$

The result (9) is shown in Fig. 3 in comparison with results of numerical simulations. We see that the tumbling rate decreases as St increases, because the coupling to the flow weakens as St increases. Finally, to order Ku^2, translational inertia does not affect the tumbling rate.

Caustics. At finite Stokes numbers the centre-of-mass motion of inertial particles exhibits caustics [27] where the phase-space manifold describing the dependence of centre-of-mass velocity upon position folds over. This gives rise to large velocity differences between close-by particles [28–31]. For non-spherical particles phase space contains angular degrees of freedom and caustics cause particles with misaligned orientation vectors to collide. Fig. 3 (right) shows the distribution of angles $\Delta\varphi$ between orientation vectors of nearby particles. At larger
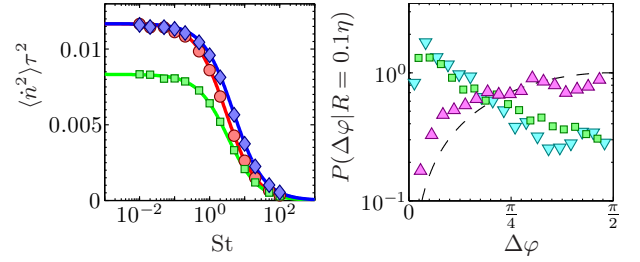
values of St caustics occur more frequently, giving rise to a broader distribution of the collision angle $\Delta\varphi$. At still larger St the distribution approaches that between uniformly randomly distributed unit vectors, $P(\Delta\varphi) = \sin\Delta\varphi$.

Conclusions. We have shown in this paper that in the absence of inertial effects, tumbling in turbulent and random flows is determined, to leading order, by Lagrangian 3-point correlations of the fluid gradients. In random flows we have computed these correlations and found that preferential effects exist but are small. In turbulent flows we have evaluated the correlation functions numerically, using the JHU turbulence data set [17, 18]. We have found that they give rise to a substantial difference in the tumbling rate between rods and disks, and have explained this difference by the fact that persistent regions of high vorticity strongly contribute to the Lagrangian three-point statistics. For larger particles, we have found that rotational inertia affects the tumbling rate and the angle at which particles collide, due to the formation of rotational caustics. It would be interesting to study how the non-ergodic statistics of vortex tubes in turbulent flows affects the tumbling rates of disks and rods with finite but small inertia.

[1] K.W. Schwarz, Phys. Rev. Lett. **64**, 415 (1990).
[2] M. Wilkinson, V. Bezuglyy, and B. Mehlig, Phys. Fluids **21**, 043304 (2009).

[3] V. Bezuglyy, B. Mehlig, and M. Wilkinson, Europhys. Lett.) **89**, 34003 (2010).

[4] M. Wilkinson, V. Bezuglyy, and B. Mehlig, J. Fluid Mech. **667**, 158 (2011).

[5] H. R. Pruppacher and J. D. Klett, *Microphysics of Clouds and Precipitation* (Springer, 1997).

[6] G. Praburam and J. Goree, Astrophys. J. **441**, 830 (1995).

[7] M. Wilkinson, B. Mehlig, and V. Uski, Astrophys. J. Suppl. Ser. **176**, 484–496 (2008).

[8] J. van Eymeren and G. Wurm, Monthly Notices of the Royal Astronomical Society **420**, 183 (2012).

[9] J. S. Guasto, R. Rusconi, and R. Stocker, Annual Review of Fluid Mechanics **44**, 373 (2012).

[10] A. Pumir and M. Wilkinson, NJP **13**, 093030 (2011).

[11] G. B. Jeffery, Proc. R. Soc. A **102**, 161 (1922).

[12] S. Parsa, E. Calzavarini, F. Toschi, and G. A. Voth, Phys. Rev. Lett. **109**, 134501 (2012).

[13] M. Shin and D. L. Koch, J. Fluid Mech. **540**, 143 (2005).

[14] D. Vincenzi, J. Fluid Mech. (2013).

[15] M. S. Chong, A. E. Perry, and B. J. Cantwell, Phys. Fluids A: Fluid Dynamics **2**, 765 (1990).

[16] M. Chertkov, A. Pumir, and B. I. Shraiman, Phys. Fluids **11**, 2394 (1999).

[17] Y. Li, E. Perlman, M. Wan, Y. Yang, C. Meneveau, R. Burns, S. Chen, A. Szalay, and G. Eyink, Journal of Turbulence p. N31 (2008).

[18] H. Yu, K. Kanov, E. Perlman, J. Graham, E. Frederix, R. Burns, A. Szalay, G. Eyink, and C. Meneveau, Journal of Turbulence (2012).

[19] B. Mehlig, M. Wilkinson, K. Duncan, T. Weber, and M. Ljunggren, Phys. Rev. E **72**, 051104 (2005).

[20] K. Gustavsson and B. Mehlig, Europhys. Lett.) **96**, 60012 (2011).

[21] K. Gustavsson and B. Mehlig, Phys. Rev. E **87**, 023016 (2013).

[22] B. Lüthi, M. Holzner, and A. Tsinober, J. Fluid Mech. **641**, 497-507 (2009).

[23] Z. S. She, E. Jackson, and S. A. Orszag, Nature **344**, 226 (1990).

[24] M. Wilkinson and H. Kennard, J. Phys. A **45**, 455502 (2012).

[25] H. Brenner, Int. J. Multiphase Flow **1**, 195 (1974).

[26] C. Marchioli, M. Fantoni, and A. Soldati, Phys. Fluids **22**, 033301 (2010).

[27] M. Wilkinson and B. Mehlig, Europhys. Lett. **71**, 186 (2005).

[28] J. Bec *et al.*, J. Fluid Mech. **646**, 527–536 (2010).

[29] K. Gustavsson and B. Mehlig, Phys. Rev. E. **84**, 045304(R) (2011).

[30] J.P.L.C. Salazar and L.R. Collins, JFM **696**, 45–66 (2012).

[31] G. P. Bewley, E. W. Saw, and E. Bodenschatz, NJP **15**, 083051 (2013).